



This is a repository copy of *Discrimination of Potent Inhibitors of Toxoplasma gondii Enoyl-Acyl Carrier Protein Reductase by a Thermal Shift Assay*.

White Rose Research Online URL for this paper:
<http://eprints.whiterose.ac.uk/110828/>

Version: Accepted Version

Article:

Afanador, G.A., Muench, S.P., McPhillie, M. et al. (16 more authors) (2013) Discrimination of Potent Inhibitors of Toxoplasma gondii Enoyl-Acyl Carrier Protein Reductase by a Thermal Shift Assay. *Biochemistry*, 52 (51). pp. 9155-9166. ISSN 0006-2960

<https://doi.org/10.1021/bi400945y>

© 2013 American Chemical Society. ACS AuthorChoice - This is an open access article published under an ACS AuthorChoice (http://pubs.acs.org/page/policy/authorchoice_termsfuse.html) which permits copying and redistribution of the article or any adaptations for non-commercial purposes.

Reuse

Unless indicated otherwise, fulltext items are protected by copyright with all rights reserved. The copyright exception in section 29 of the Copyright, Designs and Patents Act 1988 allows the making of a single copy solely for the purpose of non-commercial research or private study within the limits of fair dealing. The publisher or other rights-holder may allow further reproduction and re-use of this version - refer to the White Rose Research Online record for this item. Where records identify the publisher as the copyright holder, users can verify any specific terms of use on the publisher's website.

Takedown

If you consider content in White Rose Research Online to be in breach of UK law, please notify us by emailing eprints@whiterose.ac.uk including the URL of the record and the reason for the withdrawal request.



eprints@whiterose.ac.uk
<https://eprints.whiterose.ac.uk/>

Published in final edited form as:

Biochemistry. 2013 December 23; 52(51): 9155–9166. doi:10.1021/bi400945y.

Discrimination of Potent Inhibitors of *Toxoplasma gondii* Enoyl-Acyl Carrier Protein Reductase by Thermal Shift Assay

Gustavo A. Afanador¹, Stephen P. Muench², Martin McPhillie³, Alina Fomovska⁴, Arne Schön⁵, Ying Zhou⁴, Gang Cheng⁶, Jozef Stec⁷, Joel S. Freundlich⁸, Hong-Ming Shieh⁹, John W. Anderson⁹, David P. Jacobus⁹, David A. Fidock¹⁰, Alan P. Kozikowski⁶, Colin W. Fishwick¹¹, David W. Rice³, Ernesto Freire⁵, Rima McLeod⁴, and Sean T. Prigge^{1,*}

¹Department of Molecular Microbiology and Immunology, Johns Hopkins Bloomberg School of Public Health, Baltimore, MD 21205, USA

²School of Biomedical Sciences, University of Leeds, Leeds, LS2 9JT, UK

³Department of Molecular Biology and Biotechnology, University of Sheffield, Sheffield, UK

⁴Department of Ophthalmology and Visual Sciences, Pediatrics (Infectious Diseases), Committees on Genetics, Immunology, and Molecular Medicine, Institute of Genomics and Systems Biology, and The College, The University of Chicago, Chicago, IL 60612, USA

⁵Department of Biology, The Johns Hopkins University, Baltimore, MD 21218, USA

⁶Drug Discovery Program, Department of Medicinal Chemistry and Pharmacognosy, University of Illinois at Chicago, Chicago, IL 60612, United States

⁷Chicago State University, College of Pharmacy, DH 203-3, 9501 South King Drive, Chicago, Illinois 60628, United States

⁸Departments of Pharmacology & Physiology and Medicine, Center for Emerging and Reemerging Pathogens, UMDNJ – New Jersey Medical School, 185 South Orange Avenue Newark, NJ 07103, USA

⁹Department of Medicinal Chemistry, Jacobus Pharmaceutical Company, Princeton, NJ 08540, USA

¹⁰Department of Microbiology & Immunology and Division of Infectious Diseases, Department of Medicine, Columbia University Medical Center, New York, NY 10032, USA

¹¹School of Chemistry, University of Leeds, Leeds, LS2 9JT, UK

Abstract

Many microbial pathogens rely on a type II fatty acid synthesis (FASII) pathway which is distinct from the type I pathway found in humans. Enoyl-Acyl Carrier Protein Reductase (ENR) is an essential FASII pathway enzyme and the target of a number of antimicrobial drug discovery efforts. The biocide triclosan is established as a potent inhibitor of ENR and has been the starting point for medicinal chemistry studies. We evaluated a series of triclosan analogs for their ability to inhibit the growth of *Toxoplasma gondii*, a pervasive human pathogen, and its ENR enzyme (TgENR). Several compounds were identified that inhibited TgENR at low nanomolar concentrations, but could not be further differentiated due to the limited dynamic range of the TgENR activity assay. Thus, we adapted a thermal shift assay (TSA) to directly measure the dissociation constant (K_d) of the most potent inhibitors identified in this study as well as inhibitors from previous studies. Furthermore, the TSA allowed us to determine the mode of action of these

*To whom correspondence should be addressed. Phone: 443.287.4822 sprigge@jhsph.edu.

compounds in the presence of NADH or NAD⁺ cofactors. We found that all of the inhibitors bind to a *Tg*ENR/NAD⁺ complex, but that they differed in their dependence on NAD⁺ concentration. Ultimately, we were able to identify compounds which bind to the *Tg*ENR/NAD⁺ complex in the low femtomolar range. This shows how TSA data combined with enzyme inhibition, parasite growth inhibition data and ADMET predictions allow for better discrimination between potent ENR inhibitors for future medicine development.

INTRODUCTION

Toxoplasma gondii is an obligate intracellular, protozoan parasite that infects about one third of the world's population, causing substantial morbidity and mortality.¹⁻⁶ The life cycle of *T. gondii* is comprised of a sexual phase that only takes place in the primary host (cats of the Felidae family), and an asexual phase that can occur in any warm-blooded animal, including humans.⁷⁻⁸ Currently there is no available vaccine to prevent infection in humans, and only the antifolate medicines sulfadiazine and pyrimethamine are typically used for treatment of *T. gondii* in humans.^{2, 9} Sulfonamides are associated with hypersensitivity, and pyrimethamine with bone marrow toxicity. Even though these medications are effective against tachyzoites, the obligate intracellular form of the parasite in the acute stage of the disease, they are ineffective against the encysted, latent bradyzoites. There is no available treatment to eliminate bradyzoites in humans.¹⁰ *T. gondii* infection in immunocompetent individuals is generally asymptomatic and self-limiting, whereas in immunocompromised people, *T. gondii* infection can cause eye and brain disease such as toxoplasmic encephalitis, chorioretinitis and in severe cases can be fatal.¹¹⁻¹² Pregnant women are especially at risk because the parasite can be transmitted from mother to fetus, and can lead to congenital toxoplasmosis that may result in abortion, neonatal death, or fetal abnormalities.^{2, 9, 13-18}

T. gondii parasites contain a plastid organelle, called the apicoplast, which harbors plant-like metabolic pathways.¹⁹ One pathway that resides in the apicoplast is the machinery for a type II fatty acid synthesis (FASII) pathway which is prokaryotic-like.²⁰⁻²¹ The FASII pathway in *T. gondii* has been shown to be essential for parasite survival making it an attractive target for drug discovery efforts.²²⁻²⁶ In malaria parasites, a similar FASII pathway is critical for liver stage development²⁷⁻²⁸ and is thought to have an important role in the synthesis of lipoic acid.²⁹ In contrast to the type II pathway, humans rely on a distinct type I pathway for bulk fatty acid synthesis, which is encoded in a single polypeptide chain.³⁰ Fatty acid biosynthesis is an iterative process involving the condensation of malonyl-CoA with a nascent fatty acid chain that is covalently bound to Acyl Carrier Protein (ACP). The enzyme Enoyl-ACP Reductase (ENR) is responsible for the final reductive step in each round of fatty acid chain elongation, the NADH-dependent reduction of trans-2-enoyl-ACP to acyl-ACP.³¹ Many inhibitors of bacterial and parasitic ENR enzymes have been previously described including diazaborines, isoniazid and triclosan.³²⁻³⁴ It has been shown that triclosan inhibits *Tg*ENR with an IC₅₀ value of less than 20 nM in an *in vitro* inhibition assay using pure recombinant *Tg*ENR.³⁵ Triclosan also inhibits growth of *T. gondii* parasites with an IC₅₀ of about 200 nM, presumably due to its inhibition of the FASII pathway.²³

Even though triclosan is a potent inhibitor of *Tg*ENR, it has limitations including poor bioavailability and impairment of muscle contractility that prevent it from being a safe and effective medicine.³⁶ Instead, triclosan has been exploited as a scaffold to generate a series of analogues, many of which are also potent inhibitors of *Tg*ENR.^{35, 37-39} In this study, we report the inhibitory properties of a set of 2', 4', 5- and 6-substituted triclosan analogues developed as inhibitors of *Plasmodium falciparum* ENR (*Pf*ENR) and *Mycobacterium tuberculosis* ENR (*Mt*InhA).^{27, 40-43} Several of these compounds inhibited *Tg*ENR at low nanomolar concentrations, the lowest concentrations that we are able to assess in our

enzymatic activity assay. To further characterize the inhibitory properties of these compounds and potent inhibitors from previous medicinal chemistry efforts^{37–38} we employed a thermal shift assay (TSA). Using this assay, we were able to confirm the mode of action for all of the compounds as binding to the *Tg*ENR/NAD⁺ complex rather than to the *Tg*ENR/NADH complex or to *Tg*ENR alone. Combined with thermodynamic parameters determined by differential scanning calorimetry, we calculated dissociation constants^{44–46} for NAD⁺ and NADH binding to *Tg*ENR as well as for inhibitor binding to the *Tg*ENR/NAD⁺ complex. The K_d values we determined range from 6 mM (for NAD⁺ binding to *Tg*ENR) to 6.3 fM (for compound 19 binding to the *Tg*ENR/NAD⁺ complex), highlighting the large dynamic range of the TSA. Consequently, TSA results combined with enzyme and parasite inhibition data provide a better basis to differentiate between potent ENR inhibitors.

MATERIALS AND METHODS

Compound Preparation and Synthesis

Compounds were designed and synthesized as described by Alan Kozikowski^{37–38} and Jacobus Pharmaceutical Inc.^{27, 40–43} The purity of compounds 1–4,⁴³ 5–10,⁴⁰ 11–14,^{41–42} 15–18,²⁷ 19–29,³⁸ and 30–32³⁷ was >95% as determined by HPLC and the identity of each compound was verified by high resolution mass spectrometry. The compounds were initially dissolved in DMSO at a concentration of 10 mM, and further diluted to required concentrations in culture media (described below). For cell proliferation assays the final concentration of DMSO was not more than 0.1%, whereas for the *in vitro* *Tg*ENR enzyme assay the DMSO concentration was 1%.

Parasite and Cell Culture

The strain of *T. gondii* parasites used in this set of experiments was a modified type I RH strain which expresses yellow fluorescent protein (RH-YFP), kindly provided by Dr. Boris Striepen (University of Georgia). Parasites were maintained in confluent monolayers of Human Foreskin Fibroblast (HFF) cells at 37 °C and 5% CO₂ in culture medium consisting of Iscove's Modified Dulbecco's Medium supplemented with 10% Fetal Calf Serum, 1% Glutamax, and 1% Penicillin-Streptomycin-Fungizone (Invitrogen).

In vitro Challenge Assay

Growth inhibition of *T. gondii* was assessed as previously described.³⁸ Host cells containing RH-YFP parasites were lysed by double passage through a 25g needle, and separated from the parasites by filtration and centrifugation. Confluent monolayers of HFF cells in 96-well plates (Falcon 96 Optilux Flat-bottom) were infected with 3,500 parasites per well. Parasites were allowed to infect host cells for one hour, after which experimental compounds and control solutions were added. Seventy-two hours later, the parasite burden was assessed by measuring relative fluorescence using a Synergy H4 Hybrid Reader (BioTek) and Gen5 1.10 software. All compounds and control solutions were tested in triplicate exemplars.

Biological replicates of each experiment were performed twice for compound 17 and three times for all other compounds. The compounds were tested in a dilution series from 10 μM to 0.01 μM concentrations as described previously.³⁸ In each assay, these results were compared with those for DMSO control and triclosan. Other internal controls included a curve obtained with varying concentrations of parasites to confirm that each assay detected differing numbers of parasites, and cultures treated with a known inhibitory concentration of pyrimethamine and sulfadiazine as a positive control. Inhibitory index was calculated as: $[\text{RFU}_{(\text{compound})} - \text{RFU}_{(\text{control fibroblasts})}] / [\text{RFU}_{(\text{DMSO control})} - \text{RFU}_{(\text{control fibroblasts})}] \times 100$. MIC₅₀ is defined as the compound concentration required to inhibit replication by 50%.

Human cell proliferation assay

Potential cytotoxic effects of the compounds were assessed using Cell Proliferation Reagent WST-1 (Roche), which measures the metabolic activity of viable cells. Confluent HFF cells in 96-well plates were treated under the same conditions as in the challenge assay described above, except that the cells were not infected with parasites. After 72 hours, the cells were incubated with WST-1 reagent for 1–2 hrs, and cell viability was assessed by measuring the absorbance at 420 nm of the final colored product, which correlates directly with cell number. All samples were tested in triplicate in at least two biological replicates.

Inhibition of TgENR activity in vitro and enzymatic assay

Recombinant TgENR was purified as described previously.⁴⁷ A 96-well plate assay was used to measure the inhibition of TgENR as described previously.^{37–38} Briefly, a SpectraMax M2 plate reader was used to monitor the activity of TgENR by consumption of NADH ($\epsilon_{340} = 6220 \text{ M}^{-1}\text{cm}^{-1}$). Reactions were carried out in a final volume of 100 μL in 96 well Corning UV plates. A reaction mixture was used containing 100 μM crotonyl-CoA (Sigma), 1 μL of DMSO (or compounds dissolved in DMSO), 5nM TgENR, 100 mM Na/K Phosphate pH 7.5 150 mM NaCl and 100 μM NADH. The enzymatic activity was determined by comparing the slopes of the absorbance curves for each well to those of the blanks in the first column of the plate. Each compound was measured in duplicate at 1 μM final concentration. Potent inhibitors (>90% inhibition at 1 μM) were further analyzed to determine IC_{50} values in triplicate. Nonlinear regression analysis was performed using GraphPad Prism software.

To calculate the K_m and k_{cat} values for NADH and Crotonyl-CoA we followed a method described previously.²⁵ The K_m and k_{cat} were determined at variable concentrations of NADH (0–0.5 mM) in triplicate and a fixed concentration of crotonyl-CoA (100 μM). The K_m and k_{cat} for Crotonyl-CoA were determined at concentrations ranging from 0.8–150 μM and a fixed concentration of NADH (100 μM). Kinetic parameters were calculated by fitting the initial velocity data to the Michaelis–Menten equation using GraphPad Prism software.

Thermal Shift Assay (TSA)

A real-time PCR (RT-PCR) instrument, in the presence of Sypro Orange (an environmentally sensitive fluorescent dye), was used to monitor the thermal unfolding of TgENR alone or in the presence of ligands. The TSA was modified from previous reports^{44–46} to measure the thermal melting temperature (T_m) of TgENR. Real-time PCR tube strips (Eppendorf) were used to hold 31 μL mixtures containing final concentrations of 2 μM TgENR, 20 μM inhibitor and 100 μM cofactor. The reactions were set up with a 28 μL mixture of TgENR and buffer (20 mM HEPES pH 7.5, 100 mM NaCl) to which 1 μL of water (or cofactor dissolved in water), 1 μL DMSO (or inhibitor dissolved in DMSO), and 1 μL of Sypro Orange (Sigma, Product Number S-5692 at a final concentration of 5X) was added. The reaction mixture was incubated in the RT-PCR machine (Applied Biosystems, Step One Plus Real-Time PCR System) for 2 minutes at 20 °C followed by 0.2 °C increases in the temperature every 10 seconds until a final temperature of 80 °C was reached. During the thermal scan, fluorescence was monitored using a pre-defined TAMRA filter in which an increase in Sypro Orange fluorescence was observed upon thermal denaturation of TgENR. The derivative of the fluorescence curve was used to determine the T_m (as seen in Figure 1). The initial T_m in the absence of ligands, but in the presence of DMSO, served as the baseline temperature (T_o) for determining temperature shifts (ΔT_m). All measurements were made in triplicate.

Calculation of binding constant (K_d)

The T_m values obtained in the TSA were used to calculate the dissociation constant (K_d) as described by Mei-Chu Lo and coworkers.⁴⁴ The dissociation constant at the melting temperature was calculated using the equation

$$K_{d(T_m)} = \frac{[L_{T_m}]}{\exp \left\{ \frac{-\Delta H_{T_0}}{R} \left(\frac{1}{T_m} - \frac{1}{T_0} \right) + \frac{\Delta C_{pT_0}}{R} \left[\ln \left(\frac{T_m}{T_0} \right) + \frac{T_0}{T_m} - 1 \right] \right\}}$$

in which T_0 is the melting temperature of *Tg*ENR with no ligands (baseline), T_m is the melting temperature of *Tg*ENR in complex with one or more ligands, R is the gas constant, ΔH is the enthalpy of protein unfolding, ΔC_p is the heat capacity change on protein unfolding, and $[L_{T_m}]$ is the free ligand concentration at T_m . The two thermodynamic parameters (ΔH and ΔC_p) were measured by Differential Scanning Calorimetry. A temperature scan of 0.33 mg/mL *Tg*ENR from 10 to 65 °C at 1 °C/min was monitored using a VP-DSC microcalorimeter (MicroCal). The change in heat capacity (ΔC_{pT_0}) of 3.8 kcal/K/mol was estimated from the difference in baselines between the baselines of the denatured and native states. The enthalpy (ΔH_{T_0}) was obtained from the area under the curve yielding a value of 228.7 kcal/mol. The dissociation constant at the melting temperature was normalized to temperature T (37 °C) using the equation

$$K_{d(T)} = \frac{K_{d(T_m)}}{\exp \left(\frac{-\Delta H_{L(T)}}{R} \left(\frac{1}{T} - \frac{1}{T_m} \right) \right)}$$

which $\Delta H_{L(T)}$ is the van't Hoff enthalpy of binding at temperature T , estimated to be -15 kcal/mol.^{44, 48}

Molecular Docking

Molecular docking studies were performed using AutoDock 4.2,⁴⁹ SwissPDB Viewer⁵⁰ and MacroModel version 8.1 (Schrodinger, LLC, New York, NY, 2012) in conjunction with the X-ray crystal structures of *T. gondii* ENR in complex with inhibitors triclosan (PDB ID: 202S)⁵¹ and benzimidazole (PDB ID: 1LX6)⁵² available from the Brookhaven Protein DataBank. A 10 Å radius of the active site was used to dock the synthesized molecules with a grid box margin of 62. All other docking parameters were left as default. The obtained docking poses were analyzed using PyMol.

RESULTS AND DISCUSSION

Parasite inhibition, host cell cytotoxicity, and inhibition of *Tg*ENR enzymatic activity

A structure-based approach was adopted by Freundlich and colleagues to develop 2', 4', 5- and 6-substituted triclosan analogues against *Pf*ENR and *Mt*InhA.^{27, 40–43} In the present study, we evaluated 18 of these analogues against *Toxoplasma gondii*. The triclosan analogues were first tested for efficacy against *T. gondii* tachyzoites *in vitro*. Triclosan was also included in the assay for a direct comparison. Type 1 RH tachyzoites that express Yellow Fluorescent Protein (RH-YFP) were used, allowing parasite proliferation to be assessed by means of a fluorometric assay, since relative fluorescence is directly correlated with parasite viability. A seventy-two hour end-point was chosen to allow slow acting compounds to take effect. Seven compounds emerged as the most effective inhibitors of *T. gondii* tachyzoites: 5, 8, 9, 10, 15, 16 and 17 (Table 1). These compounds demonstrated an

efficacy equivalent to triclosan (MIC₅₀ of 2.8 μM), with MIC₅₀ values ranging from 1.6–3.5 μM. The compounds were also tested for cytotoxic activity against Human Foreskin Fibroblast host cells and exhibited no cytotoxic effects at the highest concentration tested (10 μM). These results demonstrate that inhibition of parasite growth at lower concentrations did not result from killing the host cells, however, since we did not reach the MIC₅₀ for inhibition of host cell proliferation, we do not know the overall selectivity of our compounds.

The triclosan analogues were also screened in duplicate at 1 μM for inhibition of *Tg*ENR in an *in vitro* inhibition assay. Those analogues with significant inhibitory activity (>90 % at 1 μM) were subsequently assayed in triplicate to determine their IC₅₀ values (Table 1). A total of six analogues were potent inhibitors of *Tg*ENR with IC₅₀ values of less than 23 nM, similar to that of triclosan (15 nM). None of the compounds with 2'-substitutions proved to have significant inhibitory activity. This result is consistent with a lack of potent activity against *Pf*ENR.⁴³ Based on the current crystal structures of *Tg*ENR and *Pf*ENR bound to triclosan,⁵¹ the 2'-triclosan analogues are unlikely to be effective since added bulk at this position will likely result in severe steric clashes with the NAD⁺ cofactor (see docking results for further details). Potent inhibitors of *Tg*ENR with IC₅₀ values in the low nanomolar range were found with substitutions at the 4'-, 5-, and 6-positions of triclosan. Previous medicinal chemistry efforts targeting *Tg*ENR led to the discovery of several potent 4'-triclosan and 5-triclosan analogues.^{37–38} The activities of 6-triclosan analogues have not previously been described against *T. gondii*. However, as shown in Table 1, 6-triclosan analogues such as 15 and 17 can be inhibitors of *Tg*ENR enzymatic activity and parasite growth.

Thermal Shift Assay (TSA)

Our current study of 18 triclosan analogues yielded six compounds with *Tg*ENR IC₅₀ values in the low nanomolar range (< 23 nM). These IC₅₀ values are similar to that of triclosan (15 nM) and approach the low nanomolar concentrations of *Tg*ENR enzyme used in our activity assay. Because of this we could not determine which of the six compounds is the most potent or how they compare to triclosan with currently available assays. In addition we have 14 inhibitors discovered in previous studies^{37–38} which also inhibit *Tg*ENR with IC₅₀ values lower than 100 nM, making 20 compounds in total. In an attempt to differentiate between these inhibitors, we adapted a thermal shift assay (TSA)^{44–46} to further characterize the binding of the compounds to *Tg*ENR.

A significant advantage of TSA over several other biophysical techniques, such as NMR, mass spectrometry or calorimetry, is that it can be done with higher throughput without requiring large amounts of protein.^{44–46, 48, 53–55} This method has been previously employed for screening conditions which stabilize proteins;^{46, 56–57} K_d calculations for proteins with one or two ligands;^{44–45, 48, 55} as well as to determine the mode of action of ligand binding.⁵⁵ Calculations of K_d values by TSA have been favorably compared to measurements done by other biophysical techniques.⁴⁴

We used the TSA to measure the melting temperature (T_m) of *Tg*ENR alone, in binary complex with NADH or NAD⁺ cofactor, or in a ternary complex with triclosan (or analogues) and NADH or NAD⁺ bound. Using a real time PCR machine to accurately control the temperature, we monitored the thermal denaturation of *Tg*ENR in the presence of the environmentally sensitive dye Sypro Orange. The TSA method consists of monitoring the fluorescence of the dye which has a higher quantum yield when it interacts with hydrophobic amino acids exposed upon *Tg*ENR unfolding. As shown in Figure 1, the derivative of the fluorescence intensity is marked by a sharp minimum at the T_m. A shift in thermal stability occurs upon formation of a ligand complex and the magnitude of the shift

in T_m depends on the affinity of the ligand for $TgENR$. The observed change in T_m ($\Delta T_m = T_m(\text{ligand}) - T_o(\text{no ligand})$) is used to calculate the binding constant (K_d) of the ligand.^{44, 46} TSA can be particularly useful for proteins such as $TgENR$ which have multiple ligand binding sites and can bind inhibitors and cofactor molecules. In cases like this, the relative stability of the protein with different combinations of ligands can be used to determine the mode of action of an inhibitor.⁵⁵

TgENR binary complex with NADH or NAD⁺

We studied the ΔT_m of $TgENR$ with increasing concentrations of NADH or NAD⁺ (Figure 2A). Each data point with a nonzero ΔT_m allowed us to calculate independent K_d values for these ligands. For NADH, K_d values of 26 μM ($\Delta T_m = 0.4$ C) and 21 μM ($\Delta T_m = 1.7$ C) were measured, and for NAD⁺ the K_d values were 6 mM ($\Delta T_m = 0.4$ C) and 6 mM ($\Delta T_m = 1.6$ C). The K_d values resulting from the larger temperature shifts are likely to be the most accurate (21 μM for NADH and 6 mM for NAD⁺). The K_d for NADH binding to $TgENR$ is similar to the value obtained for $PfENR$ with a K_d for NADH of 51.6 μM ⁵⁸ and that of *E. coli* ENR with a K_d for NADH of 5.4 μM .³² The K_d for NAD⁺ could not be determined for $PfENR$, except in the presence of triclosan, yielding an artificially low value of 15 μM ⁵⁸, whereas the K_d of NAD⁺ for *EcENR* was determined to be 1.8 mM.³² The kinetic parameters for $TgENR$ were calculated by using the enzymatic activity assay at 11 different concentrations of NADH and Crotonyl-CoA in triplicate, with the highest concentration of 500 μM and dilutions by factors of two for NADH and 0.8–150 μM for Crotonyl-CoA. Figure 2B shows a Michaelis-Menten plot for $TgENR$ with a k_{cat} of 12 s^{-1} and K_m of 20 μM for NADH; for Crotonyl-CoA, k_{cat} is 26 s^{-1} and K_m is 40 μM (Figure 2C). These values are similar to those of ENR enzymes from the apicomplexan parasites *Eimeria tenella* and *Plasmodium falciparum* (Table 2).^{25, 59–60} Although K_m values cannot be equated with dissociation constants, the K_m values for NADH are consistent with the 21 μM K_d value determined by TSA.

Inhibitor mode of action determined by TSA

The mode of action of ENR inhibition by triclosan has been well studied in several systems, including apicomplexan parasites, plants and bacteria. Triclosan is an uncompetitive inhibitor with respect to NAD⁺ and forms a tight ternary triclosan/NAD⁺/ENR complex. Consistent with this mechanism of action, we observed a large shift in T_m when $TgENR$ was analyzed by TSA in the presence of triclosan and NAD⁺, but not in the absence of the cofactor (Figure 1A). Interestingly, we also observed a small shift in T_m when triclosan was added to $TgENR$ in the presence of NADH (Figure 1A). Triclosan has an apparent K_d value of 186 μM for the $TgENR$ /NADH complex, an affinity that is probably too weak to have physiological significance since this value is 100,000 times larger than the K_d of triclosan binding to the $TgENR$ /NAD⁺ complex (1.3 nM at 100 μM NAD⁺ listed in Table 3). The apparent weak binding of triclosan to the $TgENR$ /NADH complex is consistent with reports of ternary triclosan/NADH complexes formed by ENR enzymes from *E. coli*,⁶¹ *Haemophilus influenza*⁶² and *Pseudomonas aeruginosa*.⁶³

Potent inhibition of ENR enzymes with triclosan is due to the slow formation of a tight ternary triclosan/NAD⁺/ENR complex. $PfENR$ is 50% identical to $TgENR$ and serves as a good example of this phenomenon. Triclosan binds to the $PfENR$ /NAD⁺ complex with relatively low affinity (53 nM) followed by the slow (0.055 s^{-1} forward rate constant) formation of a tight binding complex with an overall inhibition constant of 96 pM.⁶⁴ The tight binding complex involves the formation of an α -helix over the inhibitor binding site, a feature that was observed in the crystal structure of $TgENR$ co-crystallized with triclosan and NAD⁺, making it very likely that triclosan inhibits $TgENR$ through the same mechanism as described for other ENR enzymes.⁵¹ The slow kinetics of inhibition appear to be

responsible for the artificially high 15 nM IC_{50} value of triclosan shown in Table 1. The IC_{50} value approaches the theoretical limit (half of the 5 nM *Tg*ENR concentration) when the enzyme is preincubated with triclosan and NAD^+ allowing the inhibitory complex to form prior to initiating the assay. In the TSA experiments, there is a total incubation time of about 30 minutes from the time the experiment is set up to the time it reaches T_m . This allows enough time for triclosan to form the tight ternary complex. To confirm this, we set up TSA experiments as explained in the Methods section, but allowed 2 hours of pre-incubation. This pre-incubation time did not affect the K_d of triclosan for the enzyme (data not shown). To determine the reproducibility of the TSA measurements, we measured the T_m in four experiments in triplicates on different days for *Tg*ENR alone, in binary complex with NADH and NAD^+ and in the ternary complex *Tg*ENR/ NAD^+ /triclosan. The standard deviation of these measurements was 0.40, 0.56, 0.36 and 0.37 degree Celsius, respectively.

All of our potent inhibitors were also tested by TSA for binding to the *Tg*ENR/ NAD^+ complex, the *Tg*ENR/NADH complex, or *Tg*ENR alone. In all cases, the inhibitors displayed a similar mode of action as that of triclosan, forming a tight complex with *Tg*ENR/ NAD^+ . Figure 1B shows the TSA results for 32, a compound that differs significantly from the structure of triclosan, but displays a similar T_m shift profile and thus the same mode of action as triclosan, binding exclusively to the *Tg*ENR/ NAD^+ complex. As shown in Figure 1, the presence of 100 μ M NAD^+ alone (orange curves) or 20 μ M inhibitor alone (green curves) does not shift the T_m of *Tg*ENR and thus, the ΔT_m observed in the presence of inhibitor and NAD^+ is due to the formation of the ternary complex.

Effect of NAD^+ concentration on inhibitor affinity

In TSA experiments we can control the concentration of the cofactors NADH and NAD^+ . By contrast, in the enzymatic assay NADH is constantly being consumed and NAD^+ is formed over the course of the reaction. For TSA, we used 100 μ M NADH, the concentration used as the starting point in the enzymatic assay. As described above, this concentration is well above the 21 μ K $_d$ of NADH, ensuring that the majority of *Tg*ENR forms a binary *Tg*ENR/NADH complex during the TSA experiments. The same is not true for NAD^+ . In the TSA experiments described above, 100 μ M NAD^+ was used whereas the K_d is 6 mM. Under these conditions, the fraction of enzyme found as a binary *Tg*ENR/ NAD^+ complex is very small (~1.6%).

We then analyzed the binding of two inhibitors, triclosan and 32, to better understand how NAD^+ concentration affects the apparent K_d values determined by TSA. We determined K_d values for both inhibitors at eight concentrations of NAD^+ ranging from 2.7 μ M to 6 mM. As shown in Figure 3A, the apparent K_d for these inhibitors decreases as the concentration of NAD^+ increases, until reaching a plateau while approaching the K_d of NAD^+ (6 mM). The apparent dissociation constant of triclosan ranges from 18 μ M (at a NAD^+ concentration of 2.7 μ M) to 20 fM (at a NAD^+ concentration of 6 mM), despite the fact that NAD^+ is in stoichiometric excess to *Tg*ENR (2 μ M) throughout this concentration range. Similarly, the K_d values for compound 32 vary from 51 μ M to 689 fM over the same range of NAD^+ concentrations. These results underscore the need to consider cofactor concentration when comparing K_d values for uncompetitive inhibitors like triclosan. For example, a K_d value of 32 nM was reported for triclosan binding to *Pf*ENR⁵⁸ which is similar to the value of 1.3 nM listed in Table 3 for *Tg*ENR. However, the K_d for *Pf*ENR was determined with 250 μ M NAD^+ and the equivalent K_d value for *Tg*ENR is 105 μ M. In a similar experiment, we determined the K_d values for triclosan and compound 32 at seven concentrations ranging from 450 nM to 333 μ M, while keeping [NAD^+] constant at 100 μ M. As expected, we found that the K_d values for both compounds decrease as we increase the inhibitor concentration (Figure 3B).

We determined the K_d values for our most potent *Tg*ENR inhibitors in the presence of 6 mM NAD^+ and compared these values with those determined at 100 μM NAD^+ (Table 3). The higher NAD^+ concentration increased the apparent affinity of all of our inhibitors, however, the factor by which the affinity increased was not uniform across the compound series (Table 3). The K_d of 25 decreased by a factor of 2,300,000 when NAD^+ concentrations were increased, whereas the K_d of 30 only decreased by a factor of 11,000. Even between similar compounds such as 28 and 29 there were differences in the dependence of K_d on NAD^+ concentrations. These differences may reflect the ability of some inhibitors to bind more tightly to *Tg*ENR in the absence of NAD^+ . In the thermodynamic cycle shown in Figure 4A, these inhibitors would have smaller K_i values and larger α values corresponding to less selectivity between binding to the *Tg*ENR/ NAD^+ complex versus *Tg*ENR alone.

We did not detect the binding of any inhibitor to *Tg*ENR when we used 20 μM inhibitor concentrations, however, K_i values could be well above this level. We screened for inhibitor binding at higher concentrations of inhibitor (111 μM and 333 μM) but found that most compounds did not have measureable binding or interfered with the TSA at these concentrations. Compound 29, however, appeared to bind with a dissociation constant (K_i) of 0.8 mM (Figure 4B). This value of K_i allows us to estimate the parameter α if we can measure the affinity of compound 29 for the $\text{E}\cdot\text{NAD}$ complex (αK_i) shown in Figure 4A. The K_d of compound 29 in the presence of 6 mM NAD^+ is 116 pM (Table 3). We can estimate αK_i using the equation for the binding of uncompetitive inhibitors

$$K_i^{\text{app}} = \alpha K_i \left(1 + \frac{K_{\text{NAD}}}{[\text{NAD}]} \right)$$

in which K_i^{app} is the observed dissociation constant of the inhibitor at any concentration of NAD^+ and K_{NAD} is the K_d of NAD^+ . Since the 6 mM concentration of NAD^+ used in the TSA equals K_{NAD} , this equation reduces to:

$$\alpha K_i = \frac{K_i^{\text{app}}}{2} = 58 \text{ pM}$$

Similar estimations of αK_i can be made for all of the compounds with measured K_d values at 6 mM NAD^+ (Table 3). The parameter α describing the selectivity of compound 29 for the binary complex would then be 7×10^{-8} . The parameter α is presumably related to the ratio of K_d values shown in Table 3 in the sense that both numbers provide an indication of how dependent an inhibitor is on binding to the binary *Tg*ENR/ NAD^+ complex. This phenomenon may help to guide the selection of the best inhibitors. The NAD^+ concentration has been measured in different cell types, including mouse erythrocytes and mammalian cells with values of 368 μM and a range of 300–800 μM , respectively.^{65–69} Although the concentration of NAD^+ in the apicoplast of *T. gondii* has not been measured, it is also likely to be well below the 6 mM K_d value. Therefore, at any given time, most *Tg*ENR molecules will not have NAD^+ bound. Indeed, the large discrepancy between the MIC_{50} values in Table 1 and the extremely tight binding properties of some of the compounds in Table 3 may be an indication that NAD^+ levels are low in the apicoplast organelle.

Inhibitor affinity to the *Tg*ENR/ NAD^+ complex

The twenty compounds that we examined by TSA all had IC_{50} values of less than 100 nM in the *Tg*ENR enzyme activity assay (Table 3). The calculated K_d values at the two NAD^+ concentrations can be used to identify the most potent compounds and how dependent inhibitor binding is on NAD^+ concentration (Table 3). A total of six compounds showed K_d

values of less than 10 nM with 100 μM NAD^+ , and less than 100 fM with 6 mM NAD^+ (5, 9, 10, 15, 19 and 27). From analyzing these compounds, it is clear that tight binding inhibitors can contain small substituents at the 4'-position (as in compound 5), the 5-position (as in compound 19), or the 6-position (as in compound 15). As described previously^{37–38}, bulky substituents at the 4'- and 5-positions are accommodated by the *Tg*ENR active site. Compound 27 contains a large isoxazole ring at the 5-position while compounds 9 and 10 contain a benzylamino moiety. The 6-position triclosan analogues have not been described previously for *Tg*ENR. We show that modifications at this position are well tolerated as seen for compounds 15 and 17 (see modeling data below).

Overall, three compounds (5, 9 and 19) appear to bind to the *Tg*ENR/ NAD^+ complex as well as triclosan or better. These compounds differ, however, in terms of how dependent the dissociation constants are on NAD^+ concentration. The ratio of K_d values determined at low and high NAD^+ concentrations is 250,000 for compound 19, whereas this ratio is only 30,000 for compound 9 (Table 3). As discussed above, the reduced dependence of compound 9 on NAD^+ concentration could reflect the ability of this compound to bind weakly to *Tg*ENR, adding an additional route to forming the ternary inhibitor/*Tg*ENR/ NAD^+ complex. By contrast, compound 19 may be more dependent on binding to a preformed *Tg*ENR/ NAD^+ complex. In this sense, compound 9 could prove to be a more exciting scaffold for further modification. Since a variety of substituents are tolerated at the 5-position, these are possible additions that could improve the properties of compound 9. Similarly, small groups such as those found in compounds 15 and 17 could be added to the 6-position.

Inhibitor Modeling

In order to further understand the different binding properties of the various inhibitors studied, molecular modeling was carried out using the *Tg*ENR crystal structure and the molecular docking software AutoDock.⁴⁹ The least effective triclosan analogues contained modifications on the B-ring at the 2'-position. The close proximity of the NAD^+ cofactor to this position on the B-ring is likely to cause a significant steric clash upon inhibitor binding (Figure 5A). The addition of a 5-methyl-3-carboxamide-isoxazole group to the A- or B-rings of triclosan resulted in a marked difference in their K_d values. The presence of this group at the 5-position on the A-ring (compound 27) produced a very potent inhibitor ($K_d = 33$ fM with 6 mM NAD^+), whereas this modification at the 4'-position on the B-ring gave inhibitor 29 with 3,500 fold less affinity ($K_d = 116$ pM with 6 mM NAD^+).

Molecular modeling was used to rationalize this difference in affinity. Modeling in AutoDock suggested that the isoxazole group, and other large substituents^{37–38} can be tolerated within the hydrophobic pocket surrounding the A-ring due to the mobile alpha helix. Conversely, the positioning of this group on the B-ring extends towards the solvent exposed entrance to the binding site, and should be able to accommodate such a substituent. However, sampling the potential ligand conformations in AutoDock exposed a steric clash between the 4'-methylisoxazole of compound 29 and Phe243 (*Tg*ENR numbering) due to the rigid nature of the 5-methyl-3-carboxamide-isoxazole group. The addition of a methylene group between the amide and isoxazole ring (compound 28) decreased the K_d by about two orders of magnitude, perhaps because the additional flexibility alleviated this steric clash.

The most promising inhibitors discovered to date have a modification at the 6-position on the A-ring. Considering the extra bulk of the nitrile (compound 15) and the hydroxymethyl (compound 17) moieties, the initial steric clash observed between these substituents and Tyr179 must be alleviated through the movement about $\text{C}\beta$. This result is corroborated through further modeling studies whereby the conserved Tyr179 residue can rotate to accommodate the 6-substituents within the heart of the binding site (Figure 5B).

CONCLUSIONS

We evaluated a series of triclosan analogues as inhibitors of *Toxoplasma gondii*. The 4'- and 5-substituted triclosan analogues are effective inhibitors of parasite growth and TgENR enzymatic activity. Compounds with modifications at the 2'-position did not show inhibitory activity against TgENR due to steric clashes with either the NAD⁺ cofactor or the top of the binding pocket. Modifications in the 6-position were well tolerated and displayed good inhibitory activity against the parasite and the TgENR enzyme. Six compounds which inhibited TgENR with IC₅₀ values in the low nanomolar range were identified, but could not be further differentiated due to the limited dynamic range of the TgENR activity assay. A thermal shift assay was employed to further characterize these compounds as well as 14 other potent inhibitors from previous studies.³⁷⁻³⁸ All 20 compounds share the same mode of action and form a ternary complex with TgENR and NAD⁺, but do not bind significantly to the TgENR/NADH complex or to TgENR alone. The apparent K_d values for the inhibitors were strongly affected by NAD⁺ concentration and reached a plateau as the NAD⁺ concentration approached the 6 mM K_d of NAD⁺. By comparing the apparent K_d values of the inhibitors at low and high NAD⁺ concentrations, we could identify potent compounds which are less dependent on NAD⁺ binding. Ultimately, we were able to identify six compounds which bind to the TgENR/NAD⁺ complex in the low femtomolar range with affinities similar to or exceeding that of triclosan (5, 9, 10, 15, 19 and 27). Additionally, four of these compounds inhibit the growth of *T. gondii* parasites with equal or better potency than triclosan (5, 9, 10 and 15). TSA data combined with enzyme inhibition and parasite growth inhibition data allow for better discrimination between potent ENR inhibitors, and therefore provide an excellent method for better selection of promising lead compounds.

Acknowledgments

FUNDING STATEMENT

This work was supported by NIH grants AI082180 (to APP, DWR, RM and STP), AI085584 (to DAF), GM056550 (to EF), and GM57144 (to EF) as well as NSF grant MCB-1157506 (to EF).

The authors thank Jurgen Bosch for helpful discussions about the TSA. SPM is supported by an MRC Career Development fellowship.

Abbreviations

acetyl-CoA	acetyl coenzyme A
ACP	acyl carrier protein
CoA	coenzyme A
ENR	enoyl-ACP reductase
FASII	type II fatty acid synthesis pathway
HFF	human foreskin fibroblasts
NADH	nicotinamide adenine dinucleotide
<i>P. falciparum</i>	<i>Plasmodium falciparum</i>
<i>T. gondii</i>	<i>Toxoplasma gondii</i>
TgENR	<i>Toxoplasma gondii</i> enoyl-ACP reductase
TPSA	topological polar surface area
Sw	solubility in water

REFERENCES

1. Hill D, Dubey JP. *Toxoplasma gondii*: transmission, diagnosis and prevention. *Clin Microbiol Infect.* 2002; 8:634–640. [PubMed: 12390281]
2. McLeod R, Boyer K, Karrison T, Kasza K, Swisher C, Roizen N, Jalbrzikowski J, Remington J, Heydemann P, Noble AG, Mets M, Holfels E, Withers S, Latkany P, Meier P. Outcome of treatment for congenital toxoplasmosis, 1981–2004: the National Collaborative Chicago-Based, Congenital Toxoplasmosis Study. *Clin Infect Dis.* 2006; 42:1383–1394. [PubMed: 16619149]
3. Boyer, K.; Marcinak, J.; McLeod, R. *Toxoplasma gondii* (Toxoplasmosis). 3rd ed. New York: Churchill Livingstone; 2009.
4. Hill D, Coss C, Dubey JP, Wroblewski K, Sautter M, Hosten T, Munoz-Zanzi C, Mui E, Withers S, Boyer K, Hermes G, Coyne J, Jagdis F, Burnett A, McLeod P, Morton H, Robinson D, McLeod R. Identification of a sporozoite-specific antigen from *Toxoplasma gondii*. *J Parasitol.* 2011; 97:328–337. [PubMed: 21506817]
5. Boyer K, Hill D, Mui E, Wroblewski K, Karrison T, Dubey JP, Sautter M, Noble AG, Withers S, Swisher C, Heydemann P, Hosten T, Babiarz J, Lee D, Meier P, McLeod R. Unrecognized ingestion of *Toxoplasma gondii* oocysts leads to congenital toxoplasmosis and causes epidemics in North America. *Clin Infect Dis.* 2011; 53:1081–1089. [PubMed: 22021924]
6. Desmonts G, Couvreur J. Congenital toxoplasmosis. A prospective study of 378 pregnancies. *N Engl J Med.* 1974; 290:1110–1116. [PubMed: 4821174]
7. Dubey JP, Lindsay DS, Speer CA. Structures of *Toxoplasma gondii* tachyzoites, bradyzoites, and sporozoites and biology and development of tissue cysts. *Clin Microbiol Rev.* 1998; 11:267–299. [PubMed: 9564564]
8. Dubey JP. The history of *Toxoplasma gondii*--the first 100 years. *J Eukaryot Microbiol.* 2008; 55:467–475. [PubMed: 19120791]
9. Remington, JS.; McLeod, R.; Thulliez, P.; Desmonts, G. *Toxoplasmosis*. 7th ed. Philadelphia: Elsevier Saunders; 2011.
10. Montoya JG, Liesenfeld O. *Toxoplasmosis*. *Lancet.* 2004; 363:1965–1976. [PubMed: 15194258]
11. Luft BJ, Remington JS. Toxoplasmic encephalitis in AIDS. *Clin Infect Dis.* 1992; 15:211–222. [PubMed: 1520757]
12. Porter SB, Sande MA. Toxoplasmosis of the central nervous system in the acquired immunodeficiency syndrome. *N Engl J Med.* 1992; 327:1643–1648. [PubMed: 1359410]
13. Swisher CN, Boyer K, McLeod R. Congenital toxoplasmosis. The Toxoplasmosis Study Group. *Semin Pediatr Neurol.* 1994; 1:4–25. [PubMed: 9422215]
14. Olariu TR, Remington JS, McLeod R, Alam A, Montoya JG. Severe congenital toxoplasmosis in the United States: clinical and serologic findings in untreated infants. *Pediatr Infect Dis J.* 2011; 30:1056–1061. [PubMed: 21956696]
15. McLeod R, Mack DG, Boyer K, Mets M, Roizen N, Swisher C, Patel D, Beckmann E, Vitullo D, Johnson D, et al. Phenotypes and functions of lymphocytes in congenital toxoplasmosis. *J Lab Clin Med.* 1990; 116:623–635. [PubMed: 2146348]
16. McGee T, Wolters C, Stein L, Kraus N, Johnson D, Boyer K, Mets M, Roizen N, Beckman J, Meier P, et al. Absence of sensorineural hearing loss in treated infants and children with congenital toxoplasmosis. *Otolaryngol Head Neck Surg.* 1992; 106:75–80. [PubMed: 1734373]
17. McAuley J, Boyer KM, Patel D, Mets M, Swisher C, Roizen N, Wolters C, Stein L, Stein M, Schey W, et al. Early and longitudinal evaluations of treated infants and children and untreated historical patients with congenital toxoplasmosis: the Chicago Collaborative Treatment Trial. *Clin Infect Dis.* 1994; 18:38–72. [PubMed: 8054436]
18. McLeod R, Khan AR, Noble GA, Latkany P, Jalbrzikowski J, Boyer K. Severe sulfadiazine hypersensitivity in a child with reactivated congenital toxoplasmic chorioretinitis. *Pediatr Infect Dis J.* 2006; 25:270–272. [PubMed: 16511396]
19. Roberts CW, McLeod R, Rice DW, Ginger M, Chance ML, Goad LJ. Fatty acid and sterol metabolism: potential antimicrobial targets in apicomplexan and trypanosomatid parasitic protozoa. *Mol Biochem Parasitol.* 2003; 126:129–142. [PubMed: 12615312]

20. McFadden GI, Reith ME, Munholland J, Lang-Unnasch N. Plastid in human parasites. *Nature*. 1996; 381:482. [PubMed: 8632819]
21. Kohler S, Delwiche CF, Denny PW, Tilney LG, Webster P, Wilson RJ, Palmer JD, Roos DS. A plastid of probable green algal origin in Apicomplexan parasites. *Science*. 1997; 275:1485–1489. [PubMed: 9045615]
22. Zuther E, Johnson JJ, Haselkorn R, McLeod R, Gornicki P. Growth of *Toxoplasma gondii* is inhibited by aryloxyphenoxypropionate herbicides targeting acetyl-CoA carboxylase. *Proc Natl Acad Sci U S A*. 1999; 96:13387–13392. [PubMed: 10557330]
23. McLeod R, Muench SP, Rafferty JB, Kyle DE, Mui EJ, Kirisits MJ, Mack DG, Roberts CW, Samuel BU, Lyons RE, Dorris M, Milhous WK, Rice DW. Triclosan inhibits the growth of *Plasmodium falciparum* and *Toxoplasma gondii* by inhibition of apicomplexan Fab I. *Int J Parasitol*. 2001; 31:109–113. [PubMed: 11239932]
24. Ben Mamoun C, Prigge ST, Vial H. Targeting the Lipid Metabolic Pathways for the Treatment of Malaria. *Drug Dev Res*. 2010; 71:44–55. [PubMed: 20559451]
25. Lu JZ, Muench SP, Allary M, Campbell S, Roberts CW, Mui E, McLeod RL, Rice DW, Prigge ST. Type I and type II fatty acid biosynthesis in *Eimeria tenella*: enoyl reductase activity and structure. *Parasitology*. 2007; 134:1949–1962. [PubMed: 17697396]
26. Mazumdar J, E HW, Masek K, C AH, Striepen B. Apicoplast fatty acid synthesis is essential for organelle biogenesis and parasite survival in *Toxoplasma gondii*. *Proc Natl Acad Sci U S A*. 2006; 103:13192–13197. [PubMed: 16920791]
27. Yu M, Kumar TR, Nkrumah LJ, Coppi A, Retzlaff S, Li CD, Kelly BJ, Moura PA, Lakshmanan V, Freundlich JS, Valderramos JC, Vilcheze C, Siedner M, Tsai JH, Falkard B, Sidhu AB, Purcell LA, Gratraud P, Kremer L, Waters AP, Schiehsler G, Jacobus DP, Janse CJ, Ager A, Jacobs WR Jr, Sacchettini JC, Heussler V, Sinnis P, Fidock DA. The fatty acid biosynthesis enzyme FabI plays a key role in the development of liver-stage malarial parasites. *Cell Host Microbe*. 2008; 4:567–578. [PubMed: 19064257]
28. Vaughan AM, O'Neill MT, Tarun AS, Camargo N, Phuong TM, Aly AS, Cowman AF, Kappe SH. Type II fatty acid synthesis is essential only for malaria parasite late liver stage development. *Cell Microbiol*. 2009; 11:506–520. [PubMed: 19068099]
29. Falkard B, Kumar TR, Hecht LS, Matthews KA, Henrich PP, Gulati S, Lewis RE, Manary MJ, Winzeler EA, Sinnis P, Prigge ST, Heussler V, Deschermeier C, Fidock D. A key role for lipoleic acid synthesis during *Plasmodium* liver stage development. *Cell Microbiol*. 2013 In press.
30. Magnuson K, Jackowski S, Rock CO, Cronan JE Jr. Regulation of fatty acid biosynthesis in *Escherichia coli*. *Microbiol Rev*. 1993; 57:522–542. [PubMed: 8246839]
31. Massengo-Tiasse RP, Cronan JE. Diversity in enoyl-acyl carrier protein reductases. *Cell Mol Life Sci*. 2009; 66:1507–1517. [PubMed: 19151923]
32. Ward WH, Holdgate GA, Rowsell S, McLean EG, Pauptit RA, Clayton E, Nichols WW, Colls JG, Minshull CA, Jude DA, Mistry A, Timms D, Camble R, Hales NJ, Britton CJ, Taylor IW. Kinetic and structural characteristics of the inhibition of enoyl (acyl carrier protein) reductase by triclosan. *Biochemistry*. 1999; 38:12514–12525. [PubMed: 10493822]
33. Rozwarski DA, Grant GA, Barton DH, Jacobs WR Jr, Sacchettini JC. Modification of the NADH of the isoniazid target (InhA) from *Mycobacterium tuberculosis*. *Science*. 1998; 279:98–102. [PubMed: 9417034]
34. Grassberger MA, Turnowsky F, Hildebrandt J. Preparation and antibacterial activities of new 1,2,3-diazaborine derivatives and analogues. *J Med Chem*. 1984; 27:947–953. [PubMed: 6379179]
35. Tipparaju SK, Muench SP, Mui EJ, Ruzheinikov SN, Lu JZ, Hutson SL, Kirisits MJ, Prigge ST, Roberts CW, Henriquez FL, Kozikowski AP, Rice DW, McLeod RL. Identification and development of novel inhibitors of *Toxoplasma gondii* enoyl reductase. *J Med Chem*. 2010; 53:6287–6300. [PubMed: 20698542]
36. Cherednichenko G, Zhang R, Bannister RA, Timofeyev V, Li N, Fritsch EB, Feng W, Barrientos GC, Schebb NH, Hammock BD, Beam KG, Chiamvimonvat N, Pessah IN. Triclosan impairs excitation-contraction coupling and Ca²⁺ dynamics in striated muscle. *Proc Natl Acad Sci U S A*. 2012; 109:14158–14163. [PubMed: 22891308]

37. Cheng G, Muench SP, Zhou Y, Afanador GA, Mui EJ, Fomovska A, Lai BS, Prigge ST, Woods S, Roberts CW, Hickman MR, Lee PJ, Leed SE, Auschwitz JM, Rice DW, McLeod R. Design, synthesis, and biological activity of diaryl ether inhibitors of *Toxoplasma gondii* enoyl reductase. *Bioorg Med Chem Lett*. 2013; 23:2035–2043. [PubMed: 23453069]
38. Stec J, Fomovska A, Afanador GA, Muench S, Zhou Y, Lai BS, El Bissati K, Hickman MR, Lee PJ, Leed SE, Auschwitz JM, Sommerville C, Woods S, Roberts C, Rice D, Prigge ST, McLeod R, Kozikowski AP. Modification of Triclosan Scaffold in Search of Improved Inhibitors for Enoyl-Acyl Carrier Protein (ACP) Reductase in *Toxoplasma gondii*. *ChemMedChem*. 2013 In press.
39. Samuel BU, Hearn B, Mack D, Wender P, Rothbard J, Kirisits MJ, Mui E, Wernimont S, Roberts CW, Muench SP, Rice DW, Prigge ST, Law AB, McLeod R. Delivery of antimicrobials into parasites. *Proc Natl Acad Sci U S A*. 2003; 100:14281–14286. [PubMed: 14623959]
40. Freundlich JS, Anderson JW, Sarantakis D, Shieh HM, Yu M, Valderramos JC, Lucumi E, Kuo M, Jacobs WR Jr, Fidock DA, Schiehsler GA, Jacobus DP, Sacchettini JC. Synthesis, biological activity, and X-ray crystal structural analysis of diaryl ether inhibitors of malarial enoyl acyl carrier protein reductase. Part 1: 4'-substituted triclosan derivatives. *Bioorg Med Chem Lett*. 2005; 15:5247–5252. [PubMed: 16198563]
41. Freundlich JS, Wang F, Tsai HC, Kuo M, Shieh HM, Anderson JW, Nkrumah LJ, Valderramos JC, Yu M, Kumar TRS, Valderramos SG, Jacobs WR, Schiehsler GA, Jacobus DP, Fidock DA, Sacchettini JC. X-ray structural analysis of plasmodium falciparum enoyl acyl carrier protein reductase as a pathway toward the optimization of Triclosan antimalarial efficacy. *J Biol Chem*. 2007; 282:25436–25444. [PubMed: 17567585]
42. Freundlich JS, Wang F, Vilcheze C, Gulten G, Langley R, Schiehsler GA, Jacobus DP, Jacobs WR Jr, Sacchettini JC. Triclosan derivatives: towards potent inhibitors of drug-sensitive and drug-resistant *Mycobacterium tuberculosis*. *ChemMedChem*. 2009; 4:241–248. [PubMed: 19130456]
43. Freundlich JS, Yu M, Lucumi E, Kuo M, Tsai HC, Valderramos JC, Karagoyozov L, Jacobs WR Jr, Schiehsler GA, Fidock DA, Jacobus DP, Sacchettini JC. Synthesis and biological activity of diaryl ether inhibitors of malarial enoyl acyl carrier protein reductase. Part 2: 2'-substituted triclosan derivatives. *Bioorg Med Chem Lett*. 2006; 16:2163–2169. [PubMed: 16466916]
44. Lo MC, Aulabaugh A, Jin G, Cowling R, Bard J, Malamas M, Ellestad G. Evaluation of fluorescence-based thermal shift assays for hit identification in drug discovery. *Anal Biochem*. 2004; 332:153–159. [PubMed: 15301960]
45. Matulis D, Kranz JK, Salemme FR, Todd MJ. Thermodynamic stability of carbonic anhydrase: measurements of binding affinity and stoichiometry using ThermoFluor. *Biochemistry*. 2005; 44:5258–5266. [PubMed: 15794662]
46. Niesen FH, Berglund H, Vedadi M. The use of differential scanning fluorimetry to detect ligand interactions that promote protein stability. *Nat Protoc*. 2007; 2:2212–2221. [PubMed: 17853878]
47. Muench SP, Prigge ST, Zhu L, Kirisits MJ, Roberts CW, Wernimont S, McLeod R, Rice DW. Expression, purification and preliminary crystallographic analysis of the *Toxoplasma gondii* enoyl reductase. *Acta Crystallogr Sect F Struct Biol Cryst Commun*. 2006; 62:604–606.
48. Pantoliano MW, Petrella EC, Kwasnoski JD, Lobanov VS, Myslik J, Graf E, Carver T, Asel E, Springer BA, Lane P, Salemme FR. High-density miniaturized thermal shift assays as a general strategy for drug discovery. *J Biomol Screen*. 2001; 6:429–440. [PubMed: 11788061]
49. Goodsell DS, Morris GM, Olson AJ. Automated docking of flexible ligands: applications of AutoDock. *J Mol Recognit*. 1996; 9:1–5. [PubMed: 8723313]
50. Guex N, Peitsch MC. SWISS-MODEL and the Swiss-PdbViewer: an environment for comparative protein modeling. *Electrophoresis*. 1997; 18:2714–2723. [PubMed: 9504803]
51. Muench SP, Prigge ST, McLeod R, Rafferty JB, Kirisits MJ, Roberts CW, Mui EJ, Rice DW. Studies of *Toxoplasma gondii* and *Plasmodium falciparum* enoyl acyl carrier protein reductase and implications for the development of antiparasitic agents. *Acta Crystallogr D Biol Crystallogr*. 2007; 63:328–338. [PubMed: 17327670]
52. Miller WH, Seefeld MA, Newlander KA, Uzinskas IN, Burgess WJ, Heerding DA, Yuan CC, Head MS, Payne DJ, Rittenhouse SF, Moore TD, Pearson SC, Berry V, DeWolf WE Jr, Keller PM, Polizzi BJ, Qiu X, Janson CA, Huffman WF. Discovery of aminopyridine-based inhibitors of bacterial enoyl-ACP reductase (FabI). *J Med Chem*. 2002; 45:3246–3256. [PubMed: 12109908]

53. Todd MJ. Affinity assays for decrypting protein targets of unknown function. *Drug Discovery Today: Technologies*. 2005; 2:267–273.
54. Cummings MD, Farnum MA, Nelen MI. Universal screening methods and applications of ThermoFluor. *J Biomol Screen*. 2006; 11:854–863. [PubMed: 16943390]
55. Lea WA, Simeonov A. Differential scanning fluorometry signatures as indicators of enzyme inhibitor mode of action: case study of glutathione S-transferase. *PLoS One*. 2012; 7:e36219. [PubMed: 22558390]
56. Vedadi M, Niesen FH, Allali-Hassani A, Fedorov OY, Finerty PJ Jr, Wasney GA, Yeung R, Arrowsmith C, Ball LJ, Berglund H, Hui R, Marsden BD, Nordlund P, Sundstrom M, Weigelt J, Edwards AM. Chemical screening methods to identify ligands that promote protein stability, protein crystallization, and structure determination. *Proc Natl Acad Sci U S A*. 2006; 103:15835–15840. [PubMed: 17035505]
57. Ericsson UB, Hallberg BM, Detitta GT, Dekker N, Nordlund P. Thermofluor-based high-throughput stability optimization of proteins for structural studies. *Anal Biochem*. 2006; 357:289–298. [PubMed: 16962548]
58. Kapoor M, Mukhi PL, Surolia N, Suguna K, Surolia A. Kinetic and structural analysis of the increased affinity of enoyl-ACP (acyl-carrier protein) reductase for triclosan in the presence of NAD⁺. *Biochem J*. 2004; 381:725–733. [PubMed: 15125687]
59. Perozzo R, Kuo M, Sidhu A, Valiyaveetil JT, Bittman R, Jacobs WR Jr, Fidock DA, Sacchettini JC. Structural elucidation of the specificity of the antibacterial agent triclosan for malarial enoyl acyl carrier protein reductase. *J Biol Chem*. 2002; 277:13106–13114. [PubMed: 11792710]
60. Kapoor M, Dar MJ, Surolia A, Surolia N. Kinetic determinants of the interaction of enoyl-ACP reductase from *Plasmodium falciparum* with its substrates and inhibitors. *Biochem Biophys Res Commun*. 2001; 289:832–837. [PubMed: 11735121]
61. Sivaraman S, Sullivan TJ, Johnson F, Novichenok P, Cui G, Simmerling C, Tonge PJ. Inhibition of the bacterial enoyl reductase FabI by triclosan: a structure-reactivity analysis of FabI inhibition by triclosan analogues. *J Med Chem*. 2004; 47:509–518. [PubMed: 14736233]
62. Marcinkeviciene J, Jiang W, Kopcho LM, Locke G, Luo Y, Copeland RA. Enoyl-ACP reductase (FabI) of *Haemophilus influenzae*: steady-state kinetic mechanism and inhibition by triclosan and hexachlorophene. *Arch Biochem Biophys*. 2001; 390:101–108. [PubMed: 11368521]
63. Lee JH, Park AK, Chi YM, Moon JH, Lee KS. Crystallization and preliminary X-ray crystallographic studies of enoyl-acyl carrier protein reductase (FabI) from *Pseudomonas aeruginosa*. *Acta Crystallogr Sect F Struct Biol Cryst Commun*. 2011; 67:214–216.
64. Kapoor M, Reddy CC, Krishnasastry MV, Surolia N, Surolia A. Slow-tight-binding inhibition of enoyl-acyl carrier protein reductase from *Plasmodium falciparum* by triclosan. *Biochem J*. 2004; 381:719–724. [PubMed: 15086316]
65. Yamada K, Hara N, Shibata T, Osago H, Tsuchiya M. The simultaneous measurement of nicotinamide adenine dinucleotide and related compounds by liquid chromatography/electrospray ionization tandem mass spectrometry. *Anal Biochem*. 2006; 352:282–285. [PubMed: 16574057]
66. Houtkooper RH, Canto C, Wanders RJ, Auwerx J. The secret life of NAD⁺: an old metabolite controlling new metabolic signaling pathways. *Endocr Rev*. 2010; 31:194–223. [PubMed: 20007326]
67. Yang H, Yang T, Baur JA, Perez E, Matsui T, Carmona JJ, Lamming DW, Souza-Pinto NC, Bohr VA, Rosenzweig A, de Cabo R, Sauve AA, Sinclair DA. Nutrient-sensitive mitochondrial NAD⁺ levels dictate cell survival. *Cell*. 2007; 130:1095–1107. [PubMed: 17889652]
68. Wilhelm F, Hirrlinger J. The NAD⁺/NADH redox state in astrocytes: independent control of the NAD⁺ and NADH content. *J Neurosci Res*. 2011; 89:1956–1964. [PubMed: 21488092]
69. Hara N, Yamada K, Shibata T, Osago H, Hashimoto T, Tsuchiya M. Elevation of cellular NAD levels by nicotinic acid and involvement of nicotinic acid phosphoribosyltransferase in human cells. *J Biol Chem*. 2007; 282:24574–24582. [PubMed: 17604275]

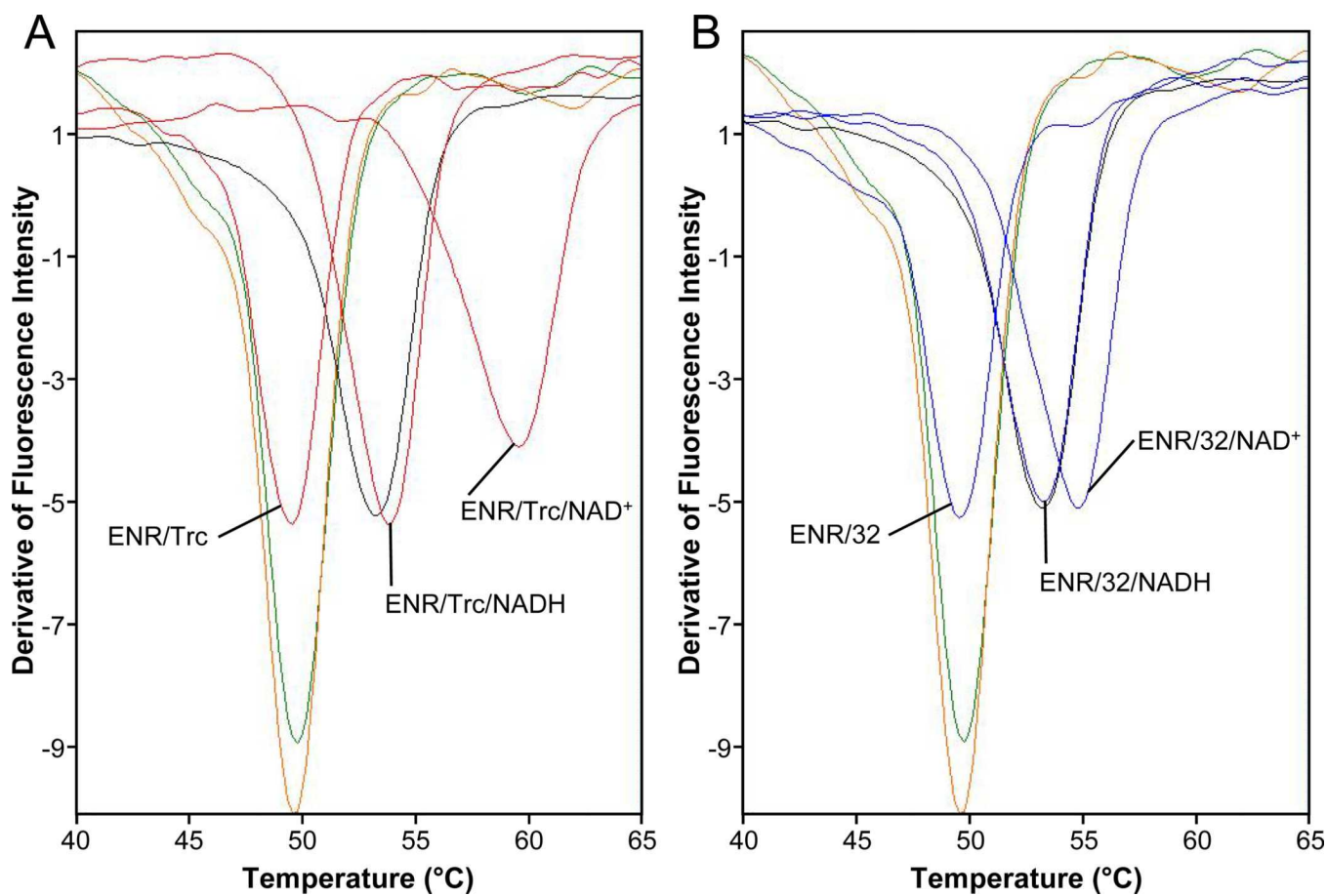


Figure 1. Thermal Shift Assay results for triclosan (red curves) and compound 32 (blue curves). The derivatives of the fluorescence intensity curves are shown with the minima defining the melting temperatures (T_m). Enzyme alone – green; Enzyme/NADH – black; Enzyme/NAD⁺ – orange.

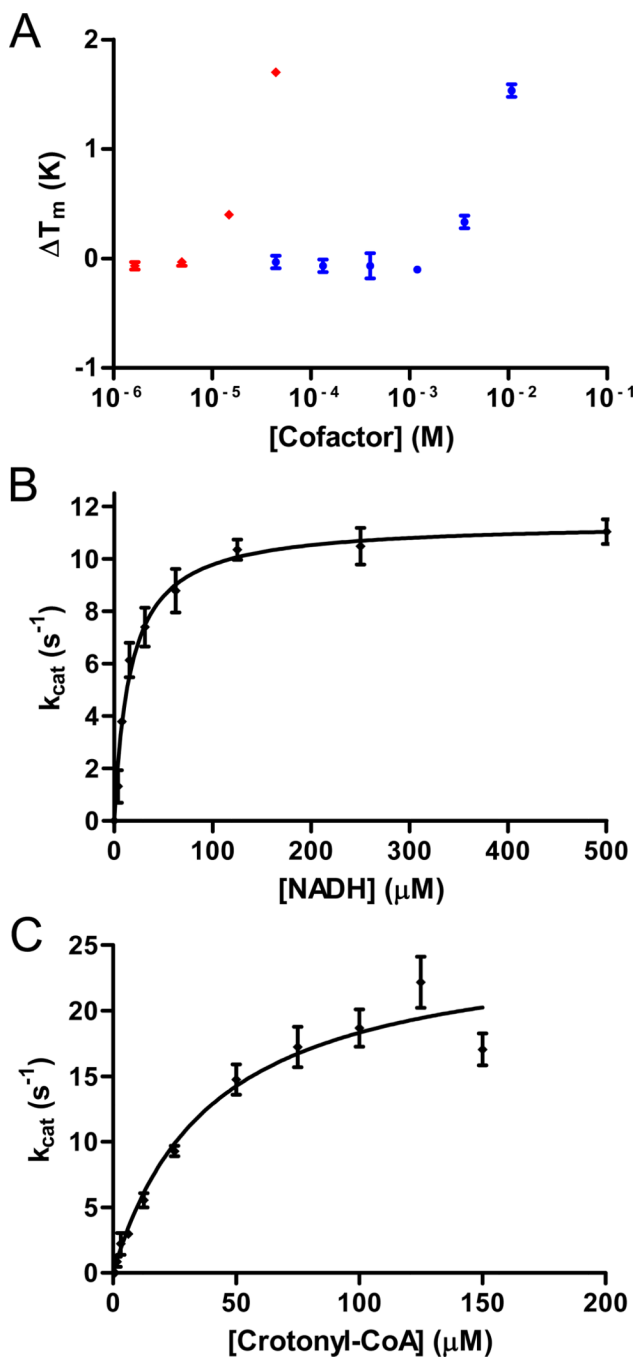


Figure 2.
A) Thermal Shift Assay results for the binding of NADH (red) and NAD⁺ (blue) to TgENR.
B) Kinetic analysis of TgENR with NADH cofactor. C) Kinetic analysis of TgENR with Crotonyl-CoA cofactor. Error bars represent the standard deviation from triplicate measurements.

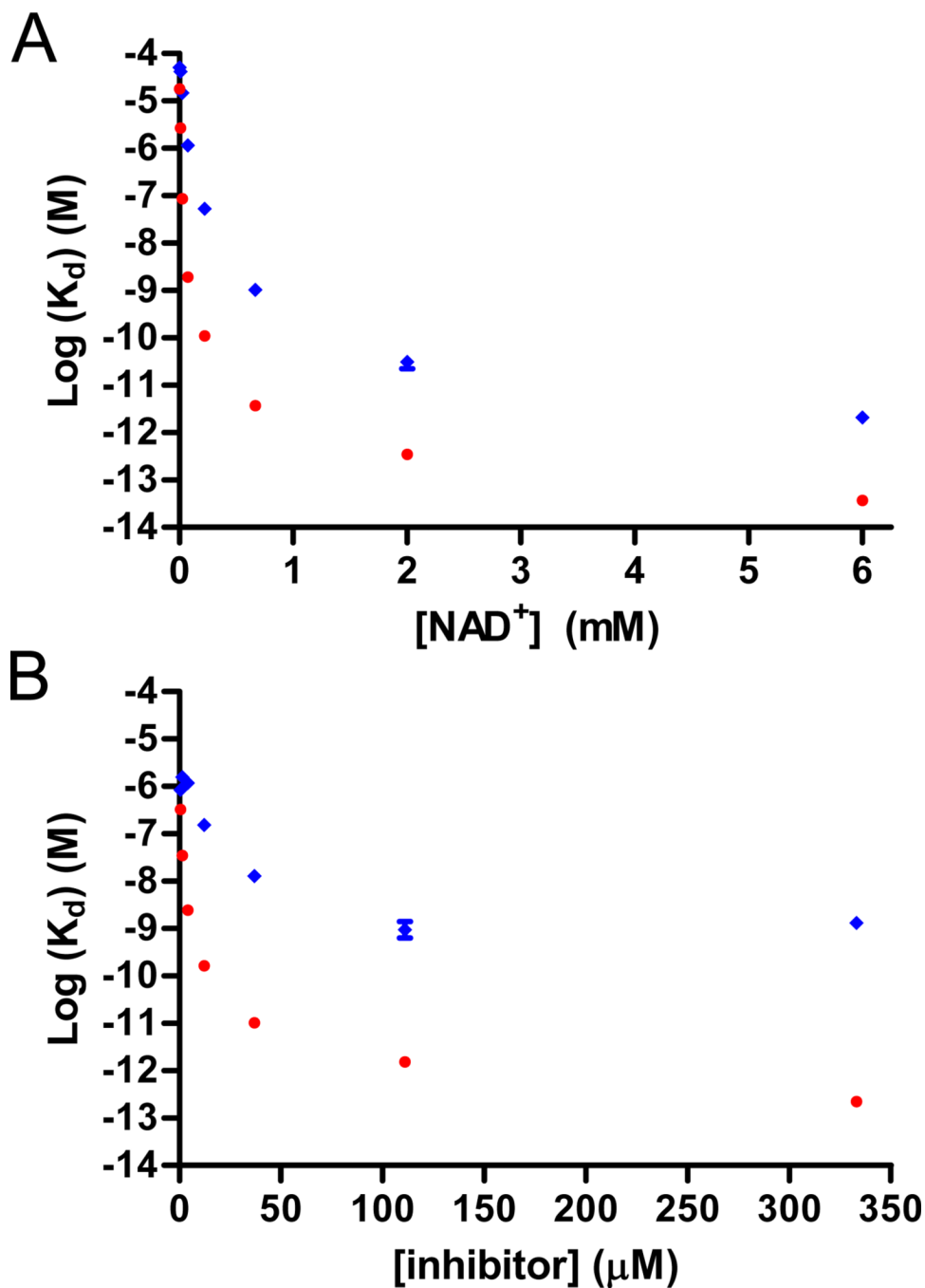


Figure 3. Effect of NAD^+ and inhibitor concentration on the apparent dissociation constant of two *TgENR* inhibitors. Thermal Shift Assay was used to determine apparent K_d values for triclosan (red) and compound 32 (blue) at different concentrations of NAD^+ and inhibitor. A) The apparent dissociation constants reach a plateau as NAD^+ concentrations approach 6 mM (the K_d of NAD^+). B) The apparent dissociation constants decrease as the inhibitor concentration increases to 333 μM , the highest concentration we were able to measure. Error bars represent the standard deviation of triplicate measurements.

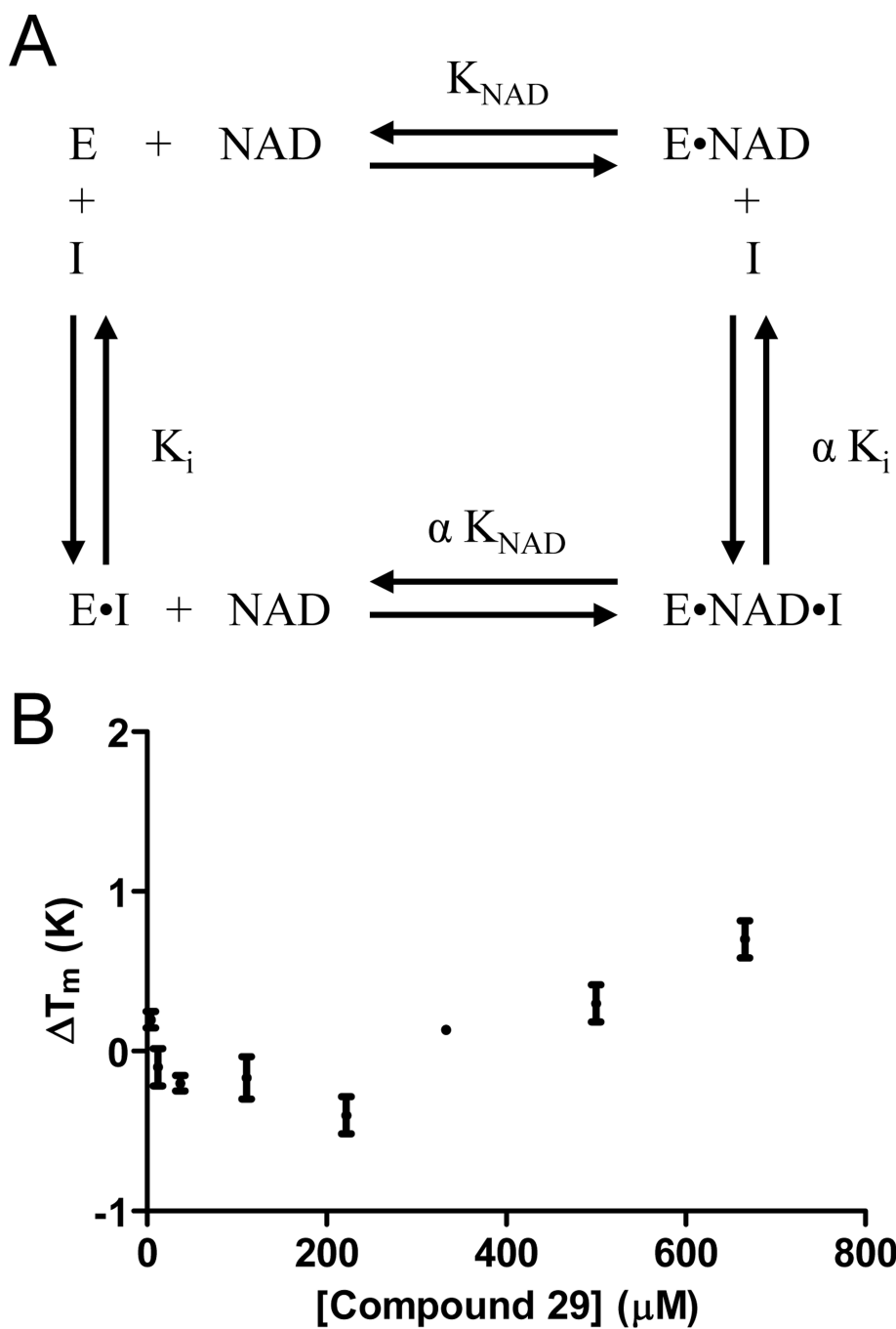


Figure 4. Thermodynamic cycle for formation of the ternary inhibitor/*Tg*ENR/ NAD^+ complex. The parameter α describes the selectivity of inhibitor binding for the *Tg*ENR/ NAD^+ complex ($E \cdot \text{NAD}$) and the selectivity of NAD^+ binding to the inhibitor/*Tg*ENR complex ($E \cdot I$).

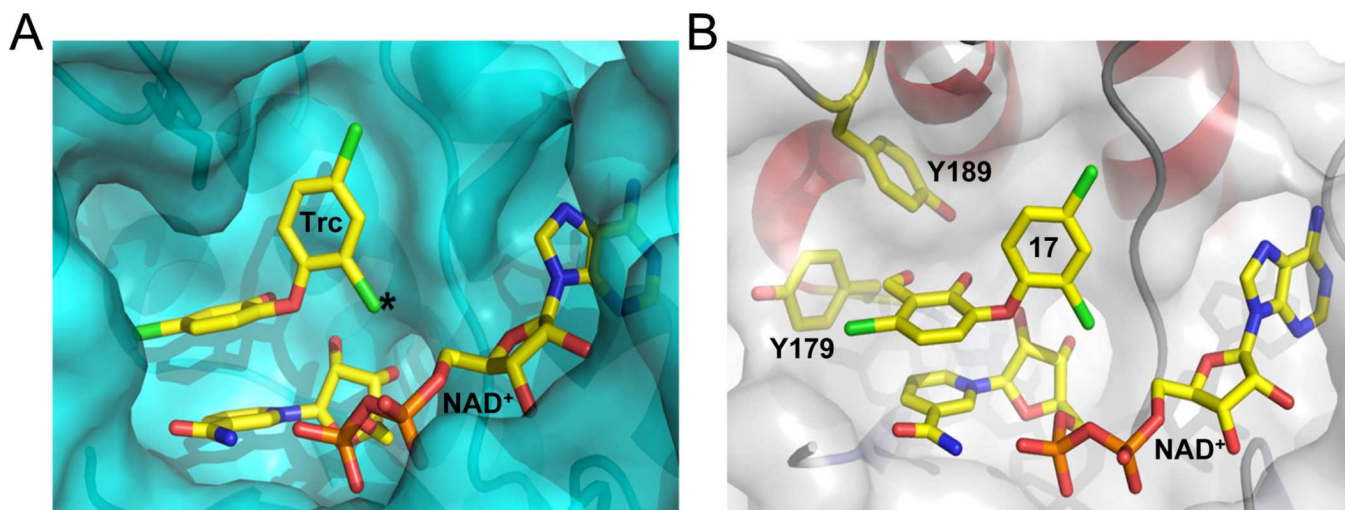
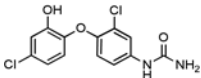
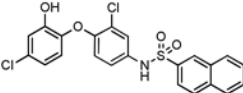
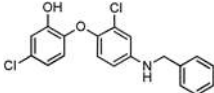
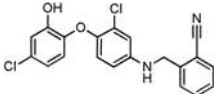
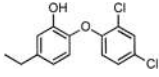
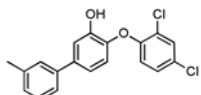
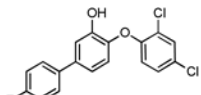
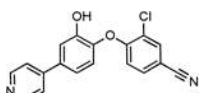


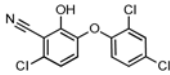
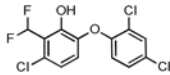
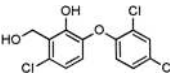
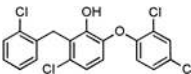
Figure 5.
A) The NAD⁺/triclosan binding pocket of *TgENR* from a crystal structure (PDB ID: 202S)⁵¹. Ligands NAD⁺ and triclosan are shown in stick format colored by atom type. Modification of the 2' atom (marked with an asterisk) results in decreased affinity (see compounds 1, 2, 3 and 4) due to steric clashes with the NAD⁺ cofactor and the binding pocket. B) Molecular modeling of inhibitor 17 showing the position of the additional OH group and its close proximity to the two fully conserved active site Tyr residues.

Table 1

Inhibitory activity, toxicity and calculated physicochemical properties of 18 substituted triclosan inhibitors of *Pf*ENR and *Mt*InhA.

Compd.	Structure	Cell Growth Inhibition		<i>Tg</i> ENR Inhibitor			Physicochemical Properties (ACD/Labs) ^e		
		<i>T. gondii</i> MIC ₅₀ (μM) ^a	HFF MIC ₅₀ (μM) ^b	Inhibition at 1 μM (%) ^c	IC ₅₀ (nM)	95% Conf. Interval (nM)	clogP ^d	TPSA [Å ²]	Sw (mg/L)
Triclosan		2.8 ± 0.2	>10	98 ± 2	15	7–33	5.53	53.25	4.6 ^f
1		>10	>10	13 ± 13	nd		5.59	84.01	2.2
2		>10	>10	14 ± 7	nd		7.46	41.49	0.52
3		>10	>10	22 ± 2	nd		6.74	41.49	0.33
4		>10	>10	28 ± 5	nd		5.63	50.72	4.2
5		3.1 ± 0.3	>10	97 ± 2	3	2–5	4.44	49.69	140
6		10	>10	73 ± 5	nd		4.09	58.56	12

Compd.	Structure	Cell Growth Inhibition		<i>Tg</i> ENR Inhibitor			Physicochemical Properties (ACD/Labs) ^e		
		<i>T. gondii</i> MIC ₅₀ (μM) ^a	HFF MIC ₅₀ (μM) ^b	Inhibition at 1 μM (%) ^c	IC ₅₀ (nM)	95% Conf. Interval (nM)	clogP ^d	TPSA [Å ²]	Sw (mg/L)
7		>10	>10	74 ± 3	nd		3.82	84.58	7.4
8		3.0 ± 0.8	>10	45 ± 4	nd		6.62	84.01	0.077
9		3.5 ± 0.4	>10	98 ± 2	13	10–16	6.06	41.19	1.0
10		1.6 ± 0.3	>10	96 ± 0	16	13–20	5.64	65.28	2.1
11		>10	>10	97 ± 1	8	7–9	5.55	29.46	2.5
12		>10	>10	78 ± 1	nd		5.82	49.69	2.8
13		>10	>10	80 ± 2	nd		5.53	49.69	4.6
14		>10	>10	41 ± 1	nd		3.82	66.14	6.9

Compd.	Structure	Cell Growth Inhibition		<i>Tg</i> ENR Inhibitor			Physicochemical Properties (ACD/Labs) ^e		
		<i>T. gondii</i> MIC ₅₀ (μM) ^a	HFF MIC ₅₀ (μM) ^b	Inhibition at 1 μM (%) ^c	IC ₅₀ (nM)	95% Conf. Interval (nM)	clogP ^d	TPSA [Å ²]	Sw (mg/L)
15		2.9 ± 0.4	>10	95 ± 1	18	16–20	5.33	53.25	7.3
16		2.7 ± 0.6	>10	87 ± 2	nd		5.67	29.46	1.9
17		2.8 ± 0.7	>10	92 ± 0	23	19–26	4.44	49.69	21
18		>10	>10	81 ± 1	nd		8.26	29.46	0.024

^a MIC₅₀ of *T. gondii* growth with SEM from assays conducted in at least two independent trials each with triplicate measurements.

^b Growth inhibition of human foreskin fibroblasts (HFF).

^c Standard deviation from duplicate measurements.

^d Calculated by ChemDraw Ultra 7.0.

^e These data were predicted by ADMET suite 5.0 (ACD/Labs). TPSA = topological polar surface area; Sw = solubility in water;

^f The actual water solubility for triclosan is 12 mg/L at 20°C, according to US EPA - Reregistration Eligibility Decision (RED) for Triclosan.

Table 2

Kinetic parameters of apicomplexan ENR enzymes.

Organism	NADH				Reference
	K _m (μ M)	Std. Error (μ M) ^b	k _{cat} (s ⁻¹)	Std. Error (s ⁻¹) ^b	
<i>Eimeria tenella</i>	60		11		Lu <i>et al.</i> ²⁵
<i>Plasmodium falciparum</i>	30		49		Perozzo <i>et al.</i> ⁵⁹
<i>Toxoplasma gondii</i> ^a	20	3.5	12	0.5	This Study ^a

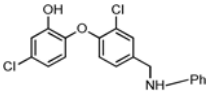
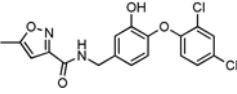
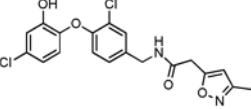
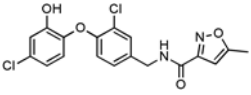
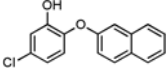
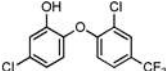
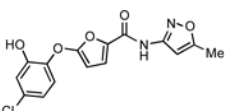
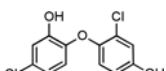
Organism	Crotonyl-CoA				Reference
	K _m (μ M)	Std. Error (μ M) ^b	k _{cat} (s ⁻¹)	Std. Error (s ⁻¹) ^b	
<i>Eimeria tenella</i>	40		6		Lu <i>et al.</i> ²⁵
<i>Plasmodium falciparum</i>	48		10		Perozzo <i>et al.</i> ⁵⁹
<i>Toxoplasma gondii</i> ^a	40	6.7	26	1.6	This Study ^a

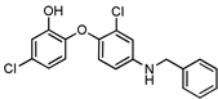
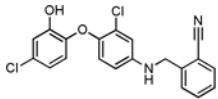
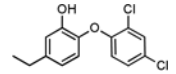
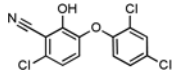
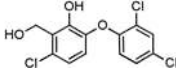
^a Kinetic measurements were determined in triplicate and the data were analyzed with GraphPad Prism software.^b Standard error as reported in GraphPad Prism software.

Table 3

Thermal shift assay results for potent inhibitors of *Tg*ENR from Table 1 and those described elsewhere.^{37–38}

Compd.	Structure	<i>Tg</i> ENR Inhibition		Thermal Shift Assay		
		IC ₅₀ (nM)	95% Conf. Interval (nM)	K _d (nM) at 100 μM ^a	K _d (fM) at 6 mM ^b	NAD ⁺ K _d Ratio ^c
Triclosan		15	13–22	1.3 ± 0.7	20 ± 3	62,000
19		24	16–36	1.6 ± 0.8	6.3 ± 1	250,000
20 ^d		38	30–48	nd	nd	nd
21 ^d		54	43–68	nd	nd	nd
22 ^d		28	22–36	nd	nd	nd
23 ^d		18	14–24	nd	nd	nd
24		26	23–41	680 ± 200	2,000 ± 300	350,000
25		43	35–54	600 ± 30	257 ± 40	2,300,000

Compd.	Structure	TgENR Inhibition		Thermal Shift Assay		
		IC ₅₀ (nM)	95% Conf. Interval (nM)	K _d (nM) at 100 μM ^a	K _d (fM) at 6 mM ^b	NAD ⁺ K _d Ratio ^c
26		31	26–37	560 ± 50	1,800 ± 400	310,000
27		19	17–21	6.9 ± 2	33 ± 5	210,000
28		33	27–40	460 ± 5	826 ± 90	550,000
29		100	79–126	19,000 ± 9,000	116,000 ± 50	170,000
30		41	31–54	9,700 ± 1,000	887,000 ± 100,000	11,000
31		30	25–34	480 ± 60	5,300 ± 2,000	90,000
32		58	42–79	440 ± 30	689 ± 40	630,000
5		3	2–5	2.1 ± 2	20 ± 1	110,000

Compd.	Structure	TgENR Inhibition		Thermal Shift Assay		
		IC ₅₀ (nM)	95% Conf. Interval (nM)	K _d (nM) at 100 μM ^a	K _d (fM) at 6 mM ^b	NAD ⁺ K _d Ratio ^c
9		13	10–16	0.8 ± 0.2	27.5 ± 6	30,000
10		16	13–20	7.3 ± 0.2	68.9 ± 70	110,000
11		8	7–9	170 ± 100	1,000 ± 3,000	170,000
15		18	16–20	9.9 ± 1	27.5 ± 6	360,000
17		23	19–26	210 ± 60	939 ± 200	220,000

^aK_d of inhibitor at a NAD⁺ concentration of 100 μM with standard deviation from triplicate measurements.

^bK_d of inhibitor at a NAD⁺ concentration of 6 mM with standard deviation from triplicate measurements.

^cRatio of K_d at 100 μM NAD⁺ to K_d at 6 mM NAD⁺.

^dThese compounds interfered with the TSA.